Recent Advances in
Petrochemical Science
ISSN: 2575-8578

Research Article
Volume 7 Issue 3 - August 2022
DOI: 10.19080/RAPSCI.2022.07.555715

Recent Adv Petrochem Sci

Nanosecond Pulse Laser Micromachining of Nickel Alloys

Z Jiang[1], AM Kamara[2]*and S Marimuthu[3]

[1]*Loughborough University, Loughborough, United Kingdom*

[2]*Department of Mechanical Engineering, University of Sierra Leone, Freetown, Sierra Leone*

[3]*The Manufacturing Technology Centre, Coventry, United Kingdom*

Submission: July 20, 2022; **Published:** August 02, 2022

***Corresponding author:** AM Kamara, Department of Mechanical and Maintenance Engineering, Fourah Bay College, University of Sierra Leone, Freetown, Sierra Leone

Abstract

Nickel alloys form a class of materials that are of great value in the manufacturing industry to produce a variety of components like gas turbine engines. However, their machining requires a technique that will ensure material removal at a rate that will facilitate the achievement of the desired finished quality. The conventional nanosecond pulse laser micromachining (PLM) has significant limitations in terms of material removal rate and eventually finished quality. Among various contributing factors to this challenge is the level of ablation, which is a consequence of the extent of the laser/material interaction during the process. Experimental investigation and numerical analysis using finite element modelling were thus carried out in this research is to examine the effect of laser power density (as an influencer of the laser intensity on the material) on the ablation depth during PLM of nickel super alloys and to identify the threshold of laser power density at which ablation could be controlled to levels that could yield appreciable finished quality. Both the experimental and the modelling results reasonably agreed that the ablation threshold for nickel super alloy occur at a laser power density of approximately 1.6 x 108 W/cm2 and above which the ablation depth increases with increase in power density and saturated at a power density of approximately 8.1×108 W/cm2. Any further increase in power density beyond this saturation value, contributes to no significant increase in ablation depth but rather cause an increase in the deterioration of the surface morphology at any scanning speed.

Keywords: Ablation; Laser; Micromachining; Nickel; Super Alloy; Finite Element Modelling

Abbreviations: PLM: Pulse Laser Micromachining; MOPA: Master Oscillator Power Amplifier; SEM: scanning electron microscope; EDX: Element Energy Dispersive X-Ray Detector.

Introduction

Nickel super alloys belong to a class of materials with extraordinary characteristics. Chiou et al. [1] identified them to have excellent mechanical properties, especially high yield strength, corrosion resistance and thermal creep resistance, which distinguished them as widely used materials in demanding applications like gas turbine engines and applications in the biomedical industry.

For the machining of this type of materials, pulse laser micromachining (either at the nanosecond, picosecond or femtosecond duration level) has become popular but with a variation in machining performance based on the level of the laser pulse duration involved. To this effect, Chichkov et al. [2] reported that, though ultrashort laser micromachining with pulse durations in the range of picosecond or femtosecond can ablate material with very little crack and recast layer, an increase in micromachining quality is also possible using femtosecond pulse durations. Further recognizing the fundamental advantage of ultrashort laser micromachining, Wei et al. [3] also revealed that its low thermal cycle and high-power density output do help to achieve a minimal recast layer.

Zheng et al. [4] used a 40W picosecond laser for the drilling of a thermal barrier coated aerospace nickel alloy as a demonstration of the performance of picosecond lasers for delamination-free hole drilling. However, depending on the laser pulse frequency, the cycle

time for the drilling of a 0.4mm diameter hole through a 1.3mm thick material ranges from 6 minutes to 2 hours. In investigating the machining of a C263 nickel superalloy using a laser operating at 10.4 ps and an average power output of approximately 3W, Semaltianos et al. [5] observed a machining throughput of ~1000 $\mu m^3/s$. Gaidys et al. [6] used a 50W picosecond laser operating at 1064nm wavelength for the machining of a copper cylinder and observed optimal machining performance at 22W with a removal rate close to $3.5mm^3/min$.

Recently Marimuthu et al. [7] used a 300W average power picosecond laser source for machining of tungsten carbide and observed a material removal rate in the range of 40-45mm^3/min with no noticeable thermal damage. Irrespective of the highlighted revelations towards ultrashort laser micromachining, various researchers including Rizvi et al. [8] have shown that the material removal rate of ultrashort pulse laser micromachining is low and the cost of machining $1cm^3$ of material by ultrashort pulse laser is extraordinarily higher than that of PLM though the lower performance level of PLM compared to the ultrashort pulse laser machining in terms of recast layer and redeposited spatter.

Williams et al. [9] further presented how the performance of PLM could be enhanced by using a master oscillator power amplifier (MOPA) based nanosecond fibre laser, which does not only have low cost and better material removal rate compared to ultrashort pulse lasers but, as reported by Yang et al. [10], is also beneficial in the control of laser pulse parameters compared to the conventional Q-switched fibre laser that has limited frequency range and unadaptable pulse duration. However, one of the biggest problems with PLM is its low micromachining quality, which is largely due to its inefficient melt ejection. As discussed by Leitz et al. [11], this effect is attributed to the continuous laser energy absorbed by the substrate melt pool in the PLM process, indicating that only a certain portion of the substrate melt can be vapourised and ejected during the process while the rest is solidified as a recast layer inside the laser machined zone. Marimuthu et al. [12] also commented on the large amount of ejected substrate melt with PLM, which is redeposited as spatter along the machined area as well as its material removal rate, which is found to be inversely proportional to the machining quality.

Notwithstanding the merits and the demerits so far highlighted about nanosecond pulse lasers relative to ultrashort pulse lasers, both the experimental and numerical investigations reported in this paper are focused on nanosecond PLM with the view to establishing the effect of laser power density (an influencer of laser intensity on the material) on ablation depth and to identify the threshold of power density with which ablation could be controlled to levels that could yield appreciable finished quality with PLM.

Experimental Setup

Experiments were performed using nanosecond PLM on a nickel superalloy with a dimension 15mm (length) × 15mm (width) × 1mm (thickness) as test material. Figure 1 shows a schematic layout of the experimental setup used. The laser source used in the experiments was a SPI MOPA pulsed fiber laser (SP-070P-A-EP-Z) [13] with a wavelength of 1.06µm, a maximum peak power of 13kW and a maximum average power of 70W. This laser source can operate with a pulse duration ranging from 10ns to 200ns. The laser system, which was equipped with a three-axis stage was such that the beam was focused using a 180mm spherical lens, and the calculated focus spot diameter was 35µm.

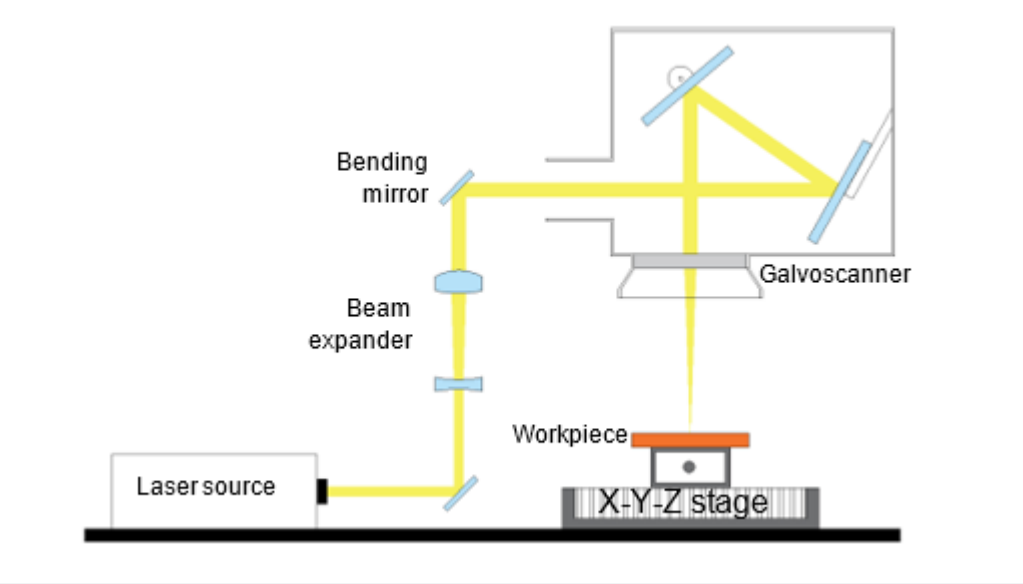

Figure 1: A schematic layout of the experimental setup used in the investigation.

How to cite this article: Z Jiang, AM Kamara, S Marimuthu. Nanosecond Pulse Laser Micromachining of Nickel Alloys. Recent Adv Petrochem Sci. 2022; 7(3): 555715. DOI: 10.19080 RAPSCI.2022.07.555715

Laser machining trials were conducted with a stationary beam and a moving stage. Samples were fixed with the coordinate stage and tests were conducted for a range of parameters. Finished samples were analyzed using optical microscope, scanning electron microscope (SEM), element energy dispersive X-ray detector (EDX) and white light interferometer.

Results

Owing to the pulse duration range of 10ns to 200ns with which the laser source in the experiments can operate, initial trial experiments were conducted to establish the most appropriate pulse duration for nanosecond PLM. Noting the potential excessive melting effect that could result with a pulse duration of 50ns or above, an arbitrary choice of lower pulse duration values of 46ns, 37ns, and 23ns was considered in investigating the effect of pulse duration and scanning speed on the ablation depth. The results of this investigation are as shown in figure 2.

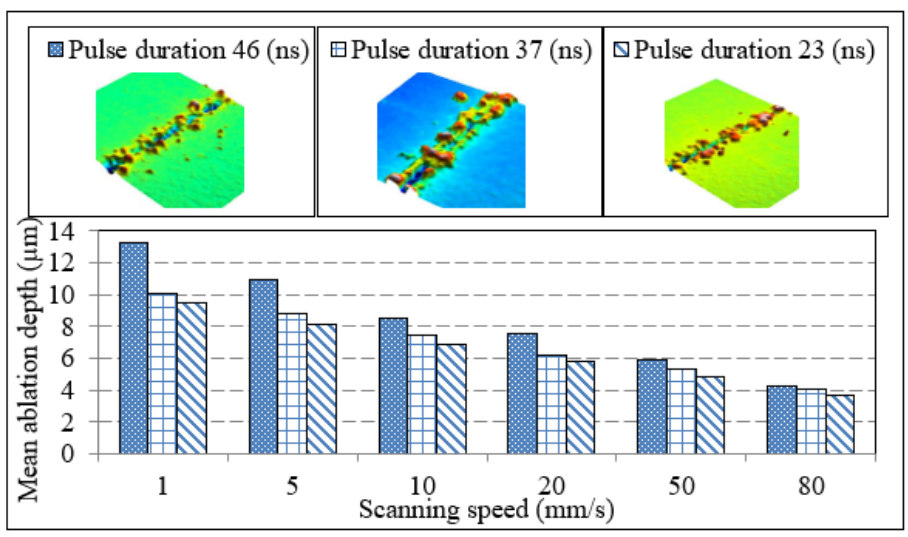

Figure 2: Effect of pulse duration and scanning speed on mean ablation depth in PLM, at a peak power of 13 kW.

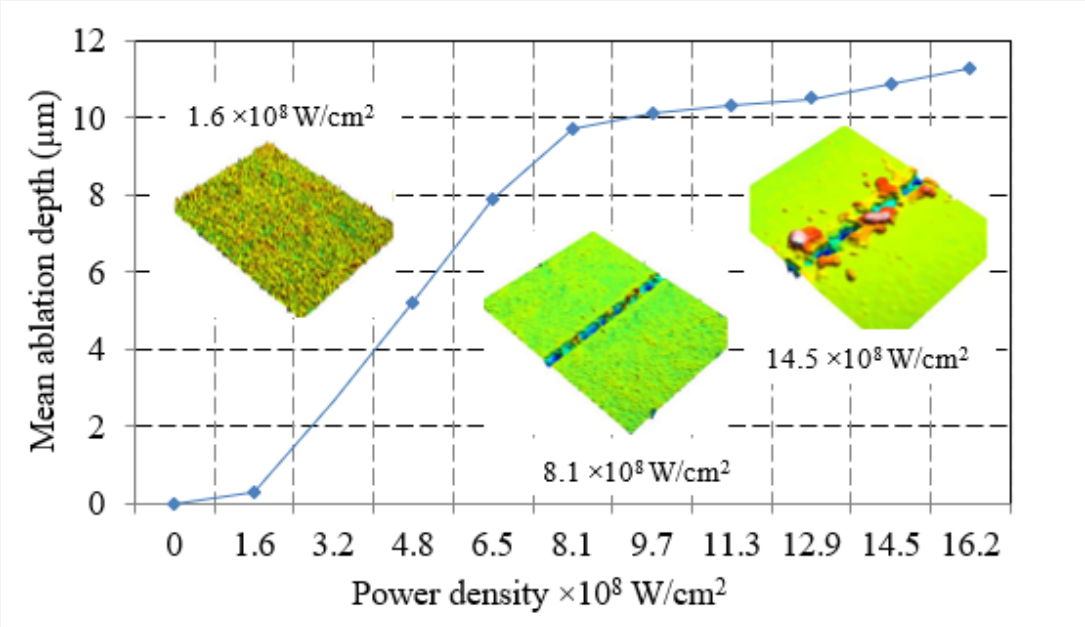

Figure 3: Effect of laser power density on mean ablation depth in PLM (speed = 5mm/s).

How to cite this article: Z Jiang, AM Kamara, S Marimuthu. Nanosecond Pulse Laser Micromachining of Nickel Alloys. Recent Adv Petrochem Sci. 2022; 7(3): 555715. DOI: 10.19080 RAPSCI.2022.07.555715

The figure shows that irrespective of the laser scanning speed, the higher the pulse duration the higher the ablation depth due to longer laser/substrate interaction with an increase in pulse duration. At a laser scanning speed of 1mm/s for instance, micromachining for a pulse duration of 46ns is shown to result in a mean ablation depth of 13.3μm while the corresponding values for pulse durations of 37ns and 23ns are 10.1μm and 9.5μm, respectively. Further shown in the figure is the gradual decrease in the mean ablation depth with increase in laser scanning speed. Also, at any given scanning speed, the laser pulse duration of 46ns exhibited the best performance in terms of the generated ablation depth and surface morphology.

Using then a pulse duration of 46ns in investigating the influence of laser power density on mean ablation depth for a constant scanning speed of 5mm/s and frequency of 105kHz, the ablation threshold of nickel superalloy as shown in figure 3, was found to occur at a power density of approximately 1.6 ×10^8 W/cm^2. Above this power density, the ablation depth is seen to increase with an increase in power density and saturated at a power density of approximately 8.1×10^8 W/cm^2. An increase in power density beyond 8.1×10^8 W/cm^2 is seen to have contributed to no significant increase in ablation depth due possibly to plasma shielding effect [14], but rather caused an increase in the deterioration of the surface morphology at any scanning speed.

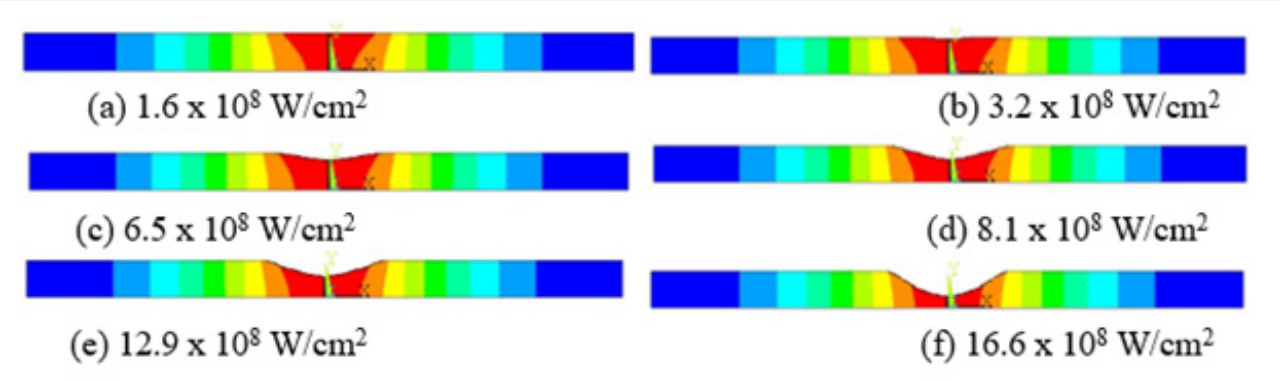

Figure 4: Variation of ablation profile (K) in PLM wih laser power density (speed =5 mm/s, number of pulse = 735, frequency = 105 kHz).

Finite Element Modelling

Using the Finite Element Modelling package ANSYS [15], a numerical analysis as discussed by Marimuthu et al. [16], was also used as a complementary investigation tool and carried out in reflection of the experimental conduct. The model used in the analysis was such that the target was represented by a mesh of finite elements that changes over time to cater for the simulation to account for the transient thermal profiles and transient ablation characteristics involved during laser micromachining. Also, varying meshes, with fine density around the laser irradiated area were used to obtain improved accuracy with the limited elements utilized. Furthermore, to moderate the computational time, a reduced domain consisting of one laser irradiated plane was used for the analysis.

The material properties used for the nickel substrate were adapted from [17] and the transient thermal problem was solved with varying boundary conditions and time steps according to the laser pulse shape and number of pulses involved. From the scanning speed of 5mm/sec, frequency of 105KHz and beam size of 35μm considered in the experimentation, the number of pulses per position used in the model was calculated as 735 following the relation:

$$\text{Number of pulse per position} = \frac{(\text{beam size x Frequency})}{(\text{Scanning speed})} \quad (1)$$

The time steps were linked to each other by using the output of time step t_s as initial condition for time step (t_s + 1) while the workpiece was assumed to have an initial temperature of 298K.

As adopted from [18], the governing equation for the two-dimensional transient heat conduction model is such that

$$pc\frac{\delta T(n,t)}{\delta t} = \frac{\delta}{\delta n}[k\frac{\delta T(n,t)}{\delta n}] + Q(t)(1-R) \quad (2)$$

where *T, t, k, p, c, Q, R,* and n denote temperature, time, thermal conductivity, density, specific heat, heat flux from laser, reflectivity, and directional vector (x, y) respectively.

During the analysis, if at the end of any time step the temperature of an element becomes higher than the melting temperature, T_m, melting is automatically assumed to have occurred and the latent heat of melting, L_m, is considered in the calculations relating to the domain represented by the melted elements. In the simulation of the PLM, vaporization/ablation is assumed to occur when the temperature of the elements is higher than the boiling temperature. Under such circumstance, the 'element death' methodology discussed in ANSYS [15] was

How to cite this article: Z Jiang, AM Kamara, S Marimuthu. Nanosecond Pulse Laser Micromachining of Nickel Alloys. Recent Adv Petrochem Sci. 2022; 7(3): 555715. DOI: 10.19080 RAPSCI.2022.07.555715

used to simulate any material removal by vaporization, with those elements representing the removed or vaporized material considered dead and having insignificant effect in the analysis of the subsequent time steps.

The heat flux Q was assumed to be a top hat distribution and was applied as a surface heat flux and worthy to note here is that the surface covered by the surface heat flux was not predetermined but rather calculated by the program in a transient manner according to the shape of the ablated profile as discussed by Marimuthu et al. [16]. Also, at the start of the simulation, the heat flux was applied over a flat surface but as the simulation progressed, the eminent material ablation does result in changes in surface geometry and consequent changes in the surface of the laser beam heat flux. The boundary condition then considered for the laser irradiated surface was

$$k\frac{\delta T}{\delta n} = Q(t)(1-R) \quad (4)$$

while that for all other surfaces was

$$k\frac{\delta T}{\delta n} = -h(T - T\infty) \quad (3)$$

where T, T_{∞} and h denote cell temperature, ambient temperature, and heat transfer coefficient respectively; and the other parameters maintaining their earlier definitions.

The simulation was performed for various power densities with the view to establishing the effect of laser power density on the ablation depth while keeping other parameters (scanning speed of 5mm/s, beam size of 35μm, frequency of 105kHz and pulse width of 46ns) constant as considered in the corresponding experimental work. For the power densities considered, figure 4 shows plots of the respective ablation depths obtained in each case, at the end of the last time step before the substrate cools down to room temperature. The simulation results as shown in the figure 4, are seen to provide a realistic view of the ablation characteristics and patterns, with an observed progressive increase in the material removed or ablated as the laser power density is increased.

A comparison of the simulation and experimental results on the effect of laser power density on ablation depth is shown in figure 5, which is a superimposition of the ablation depths in figure 4 onto the experimental results in figure 3. Both results do show very good compromise in the variation of ablation depth with laser power density up to a laser power density of approximately 8.1 x 10^8 W/cm^2. However, by the experimental results, this laser power density is portrayed as the point at which the ablation depth attained saturation since above this value of laser power density, no significant increase in ablation depth is noticed for any further increase in laser power density.

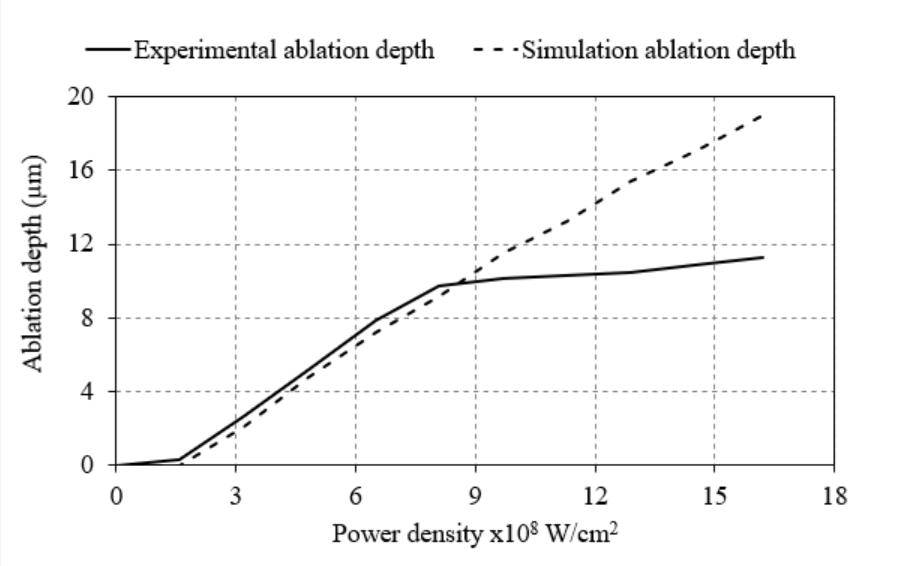

Figure 5: Variation of ablation depth in PLM with laser power density (speed =5 mm/s frequency = 105 kHz).

On the contrary, above the laser power density of 8.1 x 10^8 W/cm^2 the simulation results rather exhibit a continuous increase in ablation depth with increase in laser power density and this could be attributed to potential difficulties with the finite element program to adequately account for the material nonlinearities more so at the temperature levels involved in laser micromachining processes.

Conclusion

As evidenced by both the conducted experiments and the complementary numerical analysis, the study reported in this paper looked into the effect of laser power density (as an influencer

How to cite this article: Z Jiang, AM Kamara, S Marimuthu. Nanosecond Pulse Laser Micromachining of Nickel Alloys. Recent Adv Petrochem Sci. 2022; 7(3): 555715. DOI: 10.19080 RAPSCI.2022.07.555715

of laser intensity on the material) on ablation during nanosecond PLM of nickel superalloy. Generally deduced from the study is that ablation increases with increase in laser power density and its threshold is at a laser power density of approximately 1.6 x 10^8 W/cm^2. Above this threshold, the ablation depth increases sharply with increase in power density and saturated at a power density of approximately 8.1×10^8 W/cm^2. Any further increase in power density beyond this saturation value, contributes to no significant increase in ablation depth but rather cause an increase in the deterioration of the surface morphology at any scanning speed. With the forgoing observations, further studies are encouraged to look into how the saturation value of power density together with appropriately established values of other process parameters could enhance the finished quality of nickel superalloy with PLM.

Acknowledgement

This study was supported by the Engineering and Physical Sciences Research Council Grant EP/L01968X/1.

References

1. Mau Sheng C, An Chou Y, Sheng Rui J, Chen Ming K (2014) High Temperature Oxidation Behavior of CM-247LC Nickel Base Superalloy. Advanced Materials Research, Trans Tech Publications 922: 61-66.
2. Chichkov BN, Momma C, Nolte S, Von Alvensleben F, Tünnermann A (1996) Femtosecond, picosecond, and nanosecond laser ablation of solids. Applied Physics A 63(2): 109-115.
3. Wei J, Ye Y, Sun Z, Liu L, Zou G (2016) Control of the kerf size and microstructure in Inconel 738 superalloy by femtosecond laser beam cutting. Applied Surface Science 370: 364-372.
4. Changlong Z, Kai Z, Hong S, Xiao feng Z, Zhenqiang Y (2020) Crack behavior in ultrafast laser drilling of thermal barrier coated nickel superalloy. Journal of Materials Processing Technology 282: 116678.
5. Semaltianos NG, Perrie W, Cheng J, French P, Sharp M, et al. (2010) Picosecond laser ablation of nickel-based superalloy C263. Applied physics A 98(2): 345.
6. Gaidys M, Žemaitis A, Gečys P, Gedvilas M (2019) Efficient picosecond laser ablation of copper cylinders. Applied Surface Science 483: 962-966.
7. Marimuthu S, Dunleavey J, Smith B (2020) High-power ultrashort pulse laser machining of tungsten carbide. Procedia CIRP 94: 829-833.
8. Rizvi NH, et al. (2001) Micromachining of industrial materials with ultrafast lasers. in Proc. ICALEO.
9. Williams E, Brousseau EB, Rees A (2014) Nanosecond Yb fibre laser milling of aluminium: effect of process parameters on the achievable surface finish and machining efficiency. The International Journal of Advanced Manufacturing Technology 74(5): 769-780.
10. Limei Yang, Wei Huang, Mengmeng Deng, Feng Li (2016) MOPA pulsed fiber laser for silicon scribing. Optics & Laser Technology 80: 67-71.
11. Karl Heinz L, Benjamin R, Yvonne R, Andreas O, Michael S (2011) Metal ablation with short and ultrashort laser pulses. Physics Procedia 12: 230-238.
12. Marimuthu S, Kamara AM, Whitehead D, Mativenga P, Li L, et al. (2011) Laser stripping of TiAlN coating to facilitate reuse of cutting tools. Proceedings of the Institution of Mechanical Engineers, Part B: Journal of Engineering Manufacture 225(10): 1851-1862.
13. SPI Laser Red Energy G4. 30-10-2021
14. Srikanth S, Hermann E, Aravinda K (1999) Energy loss in the plasma during laser drilling. Journal of Physics D: Applied Physics 32(14): 1605.
15. Madenci E, Guven I (2006) The finite element method and applications in engineering using ANSYS, Springer-Verlag, New York.
16. Marimuthu S, Kamara AM, Sezer HK, Li L, Ng GKL (2014) Numerical investigation on laser stripping of thermal barrier coating. Computational Materials Science 88: 131-138.
17. Everhart J (2012) Engineering properties of nickel and nickel alloys, Springer Science & Business Media, New York.
18. Paek UC, Kestenbaum A (1973) Thermal analysis of thin film micromachining with lasers. Journal of Applied Physics 44(5): 2260-2268.

DOI: 10.19080 RAPSCI.2022.07.555715

How to cite this article: Z Jiang, AM Kamara, S Marimuthu. Nanosecond Pulse Laser Micromachining of Nickel Alloys. Recent Adv Petrochem Sci. 2022; 7(3): 555715. DOI: 10.19080 RAPSCI.2022.07.555715